1-1-2016

Two-dimensional cobalt-/nickel-based oxide nanosheets for high-performance sodium and lithium storage

Dan Zhang
University of Wollongong, Zhejiang University, dz966@uowmail.edu.au

Wenping Sun
University of Wollongong, wenping@uow.edu.au

Zhihui Chen
Zhejiang University

Yu Zhang
University of Wollongong, azhang@uow.edu.au

Wenbin Luo
University of Wollongong, wl368@uowmail.edu.au

See next page for additional authors

Two-dimensional cobalt-/nickel-based oxide nanosheets for high-performance sodium and lithium storage

Abstract

Two-dimensional (2D) nanomaterials are one of the most promising types of candidates for energy-storage applications due to confined thicknesses and high surface areas, which would play an essential role in enhanced reaction kinetics. Herein, a universal process that can be extended for scale up is developed to synthesise ultrathin cobalt-/nickel-based hydroxides and oxides. The sodium and lithium storage capabilities of Co3O4 nanosheets are evaluated in detail. For sodium storage, the Co3O4 nanosheets exhibit excellent rate capability (e.g., 179 mA h g¿1 at 7.0 A g¿1 and 150 mA h g¿1 at 10.0 A g¿1) and promising cycling performance (404 mA h g¿1 after 100 cycles at 0.1 A g¿1). Meanwhile, very impressive lithium storage performance is also achieved, which is maintained at 1029 mA h g¿1 after 100 cycles at 0.2 A g¿1. NiO and NiCo2O4 nanosheets are also successfully prepared through the same synthetic approach, and both deliver very encouraging lithium storage performances. In addition to rechargeable batteries, 2D cobalt-/nickel-based hydroxides and oxides are also anticipated to have great potential applications in supercapacitors, electrocatalysis and other energy-storage-/-conversion-related fields.

Keywords

two-dimensional, nanosheets, storage, high-performance, sodium, lithium, cobalt-/nickel-based, oxide

Disciplines

Engineering | Physical Sciences and Mathematics

Publication Details

Zhang, D., Sun, W., Chen, Z., Zhang, Y., Luo, W., Jiang, Y. & Dou, S. Xue. (2016). Two-dimensional cobalt-/nickel-based oxide nanosheets for high-performance sodium and lithium storage. Chemistry - A European Journal, 22 (50), 18060-18065.

Authors

Dan Zhang, Wenping Sun, Zhihui Chen, Yu Zhang, Wenbin Luo, Yinzhu Jiang, and Shi Xue Dou

Two-dimensional Cobalt/Nickel-Based Oxide Nanosheets for High-Performance Sodium and Lithium Storage

Dan Zhang,[a,b] Wenping Sun,*[b] Zhihui Chen,[a] Yu Zhang,[b] Wenbin Luo,[b] Yinzhu Jiang,*[a] Shi Xue Dou[b]

Abstract: Two-dimensional (2D) nanomaterial is one of the most promising candidates for energy storage applications due to its confined thickness and high surface area, which would play an essential role for enhanced reaction kinetics. In this work, a universal process that can be extended to scale-up is developed for synthesizing ultrathin Co/Ni-based hydroxides and oxides. The sodium and lithium storage capability of Co_3O_4 nanosheets are evaluated in detail. For sodium storage, the Co_3O_4 nanosheets exhibit excellent rate capability (e.g. 179 mA h g^{-1} at 7.0 A $g^{-1}$and 150 mA h g^{-1} at 10.0 A g^{-1}) and promising cycling performance (404 mA h g^{-1} after 100 cycles at 0.1 A g^{-1}). Meanwhile, very impressive lithium storage performance is also achieved, which maintains 1029 mA h g^{-1} after 100 cycles at 0.2 A g^{-1}. NiO and $NiCo_2O_4$ nanosheets are also successfully prepared with the same synthesis approach, and both deliver very encouraging lithium storage performance. In addition to rechargeable batteries, the 2D Co/Ni-based hydroxides and oxides are also anticipated to have great potential applications in supercapacitors, electrocatalysis, and other energy storage/conversion-related fields.

Introduction

Two-dimensional (2D) nanomaterials are highly desirable for energy storage and conversion, electronics, photocatalysis, biosensing, *etc.*, due to their exciting physical, chemical or electronic properties, which can be attributed to their confined atomic thickness, high specific surface area and quantum confinement of electrons in 2D plane. [1] Enormous progresses of graphene-based 2D nanostructures have been achieved in various applications in the past decade.[2] These achievements have sparked numerous interests of 2D inorganic compounds, such as metal oxides, metal chalcogenides and others .[3]

Lithium/sodium ion batteries (LIBs/SIBs) are springing rapidly as new generation devices for energy storage systems as well as electric vehicles.[4] Transition metal oxides (TMOs) and chalcogenides (TMCs) stand out as promising alternative anode candidates for LIBs/SIBs due to the higher theoretical capacity based on the conversion reaction mechanism.[5] However their practical use is impeded by poor cycling stability caused by inevitable volume change and the sluggish reaction kinetics.[5a, b, 6] In regarding to sodium storage, the sluggish reaction kinetics becomes more significant, and hence the delivered capacities are much lower than the theoretical values.[4a] In order to address these issues, tremendous effort has been devoted to developing more efficient and robust electrode materials with various nanostructures, such as nanospheres, nanofibers, nanoflakes, nanosheets, and so forth.[5c, 7] 2D nanosheet is one of the most efficient nanostructures for enhanced lithiation/delithiation or sodiation/desodiation reactions, which can provide significantly shortened ion and electron diffusion pathway, sufficient electrode/electrolyte contact, abundant electrochemical active sites and high mechanical flexibility to endow long-term cycling stability.[3a, d, 8]

Driven by the fascinating properties and promising applications, much effort has been devoted to exploring various kinds of synthetic strategies to produce 2D nanomaterials.[9] So far, a scalable and cost-effective approach to prepare homogenous especially large-area 2D inorganic nanomaterials (e.g., metal oxides nanosheets), is still a great challenge. At early stages, 2D nanostructures are dominantly obtained via the exfoliation method, in which single or few-layer structures are generated by intercalating metal ions or solvent molecules into the parent layered structures. Although exfoliation represents a versatile and scalable route, it is usually uncontrollable in terms of the uniformity of size/shape, thickness and lateral dimension.[10] Another popular method to fabricate 2D nanomaterials is high-temperature chemical vapour deposition (CVD), which favours the synthesis of 2D nanomaterials with high quality and purity. However, CVD is closely dependent on the substrate accompanied with low yield and high cost.[11] Oil-phase synthesis with capping agent is a low-cost and highly reliable process, which can efficiently produce 2D transition metal chalcogenide with fewer defects and less crystalline disorder than other methods. However, it is not easy to obtain the desired stoichiometry and is very hard to be scaled up. [9a, 12]

Herein, we report a facile and scalable approach to synthesize high-quality 2D Co_3O_4 nanosheets under mild hydrothermal reactions followed by a quick heat treatment process. The nanosheet morphology is well inherited from the layered structured 2D $Co(OH)_2$ nanosheets. Notably, this approach could be extended to the synthesis of other analogue nanosheets including binary and ternary transition metal oxides (NiO and $NiCo_2O_4$). As anode materials for LIBs/SIBs, the 2D nanosheets show extraordinary electrochemical performance in terms of specific capacity, rate capability and cycling life.

[a] Dr . D. Zhang, Z. Chen, Prof. Y. Jiang
State Key Laboratory of Silicon Materials, Key Laboratory of Advanced Materials and Applications for Batteries of Zhejiang Province and Department of Materials Science and Engineering, Zhejiang University
Hangzhou, Zhejiang 310027(P. R. China)
E-mail: yzjiang@zju.edu.cn
[b] Dr. D. Zhang, W. Sun, Y. Zhang, W. Luo, Prof. S. X. Dou
DepartmentInstitute for Superconducting and Electronic Materials, University of Wollongong
Wollongong, NSW 2522 (Australia)
E-mail: wenping@uow.edu.au
Supporting information for this article is given via a link at the end of the document.

Results and Discussion

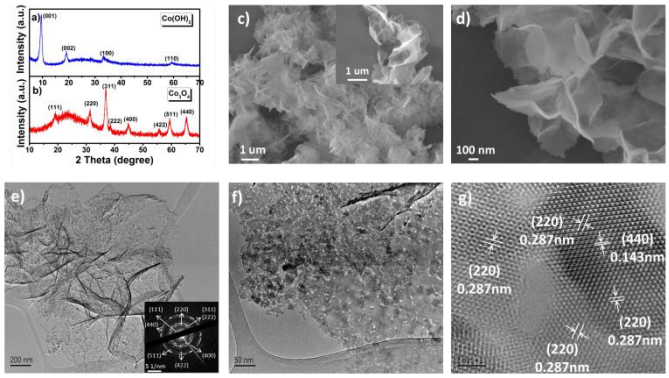

Figure 1. Figure Caption. XRD patterns of as-prepared products: (a) $Co(OH)_2$ and (b) Co_3O_4. SEM images of as-prepared products: (c) $Co(OH)_2$ and (d) Co_3O_4. (e) TEM, (f) High magnification TEM and (g) HRTEM image of Co_3O_4 nanosheets. The inset in Fig. 1c and e is the high magnification SEM image and SAED pattern, respectively.

Figure 1a shows the X-ray diffraction (XRD) result of the as-prepared product synthesized by the solvothermal process at 120 °C for 4 h. All the diffraction peaks can be indexed to hexagonal layered *α*-$Co(OH)_2$ (JCPDS card no. 51-1731). Figure 1c shows that *α*-$Co(OH)_2$ possesses graphene-like 2D morphology. From the inset of Figure 1c, we can see that the nanosheets are uniform and in micron plane size. The crumple of the nanosheets can be ascribed to the consequence of accommodating the excessive surface energy. The thermal gravimetric analysis (TGA) curve of the *α*-$Co(OH)_2$ nanosheets are presented in Figure S1, which demonstrates two stages of weight loss within the temperature range of 50-450 °C. The weight loss below 175 °C is associated with the evaporation of absorbed water. The major weight loss occurs within the temperature range of 175-450 °C, which is related to the decomposition and oxidization of *α*-$Co(OH)_2$ to Co_3O_4. According to the TGA result, the nominal formula of the as prepared product is calculated to be $Co(OH)_2 \cdot 0.5H_2O$. Figure 1b shows the XRD pattern of the product after calcining *α*-$Co(OH)_2$ at 300 °C for 2h. All the diffraction peaks are consistent with a cubic phase structure of Co_3O_4 (JCPDS Card NO. 65-3103). As shown in Figure 1d, the Co_3O_4 inherits the nanosheet morphology of *α*-$Co(OH)_2$, indicating the 2D graphene-like morphology can be well preserved after the mild heat treatment process. The TEM image shown in Figure1e further confirms the ultrathin characteristic as well as a typically wrinkle structure of Co_3O_4 nanosheets. The corresponding selected area electron diffraction (SAED) pattern (inset of Figure 1e) reveals the polycrystalline nature of the nanosheets, which can be indexed to (111), (220), (311), (222), (400), (422), (511) and (440) planes of cubic Co_3O_4, and is in high agreement with the XRD result. The high magnification TEM image in Figure 1f depicts the detailed morphology of one single nanosheet constructed with numerous nanoparticles and uniform nanosized holes (2-10 nm), which will provide high surface areas for electrolyte/electrode contact and sufficient space for releasing the strain caused by volume changes over cycling. The high resolution TEM (HRTEM) image (Figure 1g) shows typical lattice fringes with interplanar distances of 0.143 and 0.287 nm, which can be assigned to the (220) and (440) planes of cubic Co_3O_4. Figure S2 shows the nitrogen adsorption–desorption isotherms and the corresponding pore size distributions of as prepared Co_3O_4 nanosheets.

To evaluate the sodium storage ability of the ultrathin Co_3O_4 nanosheets, coin-type half cells were assembled and a series of electrochemical measurements were carried out at room temperature. Cyclic voltammetry (CV) test of the cell was conducted at 0.1 mV s^{-1} in the voltage range of 0.01-3.0 V (vs. Na/Na^+) (Figure 2a). During the initial cathodic scan, two broad reduction peaks appear. The cathodic peak at ~1.03 V disappearing in the following cycles could be ascribed to the formation of an irreversible solid electrolyte interphase (SEI) layer. Another cathodic peak at ~0.47 V in the first cycle corresponds to the reduction of Co_3O_4 to metallic Co accompanied by the electrochemical formation of Na_2O. In the following anodic scan, there is a broad peak at ~1.63 V, which is related to the re-oxidation of Co to Co_3O_4 and decomposition of Na_2O. Theoretically, sodium storage is achieved by the conversion reaction for Co_3O_4, with the formation of Co and Na_2O (sodiation reaction) and the reformation of Co_3O_4 (desodiation reaction) as described by the following electrochemical reaction.[13]

$Co_3O_4 + 8\ Na^+ + 8e^- \leftrightarrow 4Na_2O + 3Co$

In the subsequent cycles, only one cathodic peak at ~0.63 V can be observed, which can be attributed to the reduction of Co_3O_4. The CV curves overlapping in the third and fourth cycles demonstrate good electrochemical stability of Co_3O_4 nanosheets over cycling.

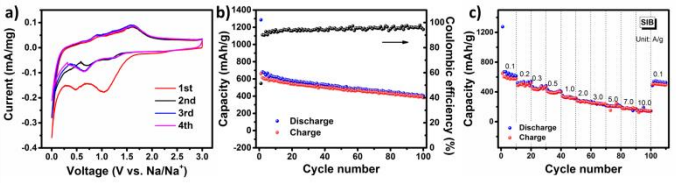

Figure 2. (a) CV curves of Co_3O_4 nanosheet electrode in the voltage window of 0.001-3.0 V (vs. Na/Na^+) at a scan rate of 0.1 mV s^{-1}. (b) Cycling performance of Co_3O_4 nanosheets as anode materials of SIB at a current density of 100 mA g^{-1}. (c) Rate capability of Co_3O_4 nanosheet electrode of SIB at different current rates in the voltage window of 0.01-3.0 V (vs. Na/Na^+).

Figure 2b presents the cycling performance of the Co_3O_4 nanosheet electrode at a current density of 100 mA g^{-1} in the voltage range of 0.01-3.0 V (vs. Na/Na^+). The first discharge capacity (1286 mA h g^{-1}) is higher than the theoretical capacity (890 mA h g^{-1}), which is generally caused by the inevitable decomposition of electrolyte and the irreversible formation of SEI.[14] Due to the significantly irreversible contribution, the first charge capacity is 661 mAh g^{-1}, showing columbic efficiency of 51.4%. The reversible capacity is lower than the theoretical value, which is in great part due to the relatively sluggish reaction (sodiation/desodiation) kinetics. However, it has to be mentioned that the reversible charge capacity is improved greatly as compared with the previous reports about Co_3O_4 anodes for sodium storage, e.g. hierarchical Co_3O_4

spheres/CNTs (487 mA h g^{-1} at 160 mA g^{-1}),[15] 39mesoporous Co_3O_4 sheets/3D graphene (375.5 mA h g^{-1} at 25 mA g^{-1}),[16] and Co_3O_4 nanopartciles@nitrogen-doped carbon (516 mA h g^{-1} at 100 mA g^{-1}).[17] The 2D ultrathin morphology should play a key role in enhancing the sodiation/desodiation reaction kinetics and thereby specific capacity. It is clearly seen that the Co_3O_4 nanosheet electrode shows promising cycling performance, and the capacity maintains to be 404 mA h g^{-1} after 100 cycles, with a capacity retention of ~60%. It is noted that the cycling stability of this work without carbon-based matrix is also extraordinary compare to the aforementioned Co_3O_4 with other nanostructures, as the Table S1 shows. The rate capability of the ultrathin Co_3O_4 nanosheet electrode is presented in Figure 2c. The electrode shows high reversible specific discharge capacity of 538, 436, 390, 332, 281, 243, and 208 mA h g^{-1} at different current densities of 0.2, 0.3, 0.5, 1.0, 2.0, 3.0 and 5.0 A g^{-1}. Even when the current density is increased to as high as 7.0 and 10.0 A g^{-1}, the reversible capacity maintains high retention of 179 and 150 mA h g^{-1}, respectively. The cell still delivers a high capacity of 533 mA h g^{-1} when the current density is reversed to 0.1 A g^{-1}. Gradually enlarged overpotential and shorten curves assigned to conversion reactions are observed as higher rates are employed, which is a common characteristic of metal oxide based electrodes (Figure S3). The encouraging electrochemical performances indicate the unique superiority of Co_3O_4 nanosheets for sodiation/desodiation reaction, which provides fast kinetics for Na^+ diffusion and charge transfer, and sufficient space for accommodating volume change.

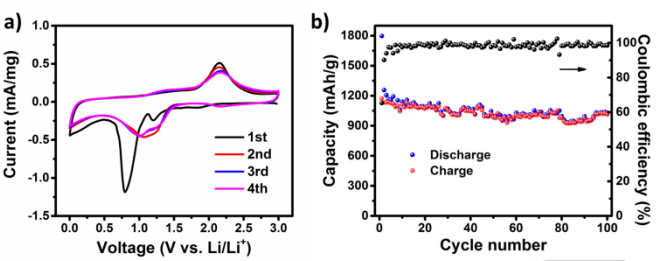

Figure 3. (a) CV curves of Co_3O_4 nanosheet electode in the voltage window of 0.001-3.0 V (vs. Li/Li^+) at a scan rate of 0.1 mV s^{-1}. (b) Cycling performance of Co_3O_4 nanosheets as anode materials of LIB at a current density of 200 mA g^{-1}.

In addition to sodium storage, the lithium storage capability of Co_3O_4 nanosheets was also evaluated with the coin-type half cells. The CV curves was tested at a scan rate of 0.1 mV s^{-1} in the voltage range of 0.01-3.0 V (vs. Li/Li^+). As shown in Figure 3a, two cathodic peaks are observed at 1.2 and 0.8V in the first cycle, which correspond to the electrochemical reduction reaction of Co_3O_4 and the formation of SEI layer. The anodic peak at 2.15V can be ascribed to the re-oxidation reaction to form Co_3O_4. The peaks in subsequent scans overlap, indicating the superiority of Co_3O_4 nanosheets as durable anode material for LIBs. It should be noted that, as compared with the case for sodium storage (Figure 2a), much intenser redox peaks are observed for lithium storage, indicating faster lithiation/delithiation reaction kinetics. The sluggish sodiation/desodiation reaction kinetic is mostly attributed to the larger ionic radius of sodium ions.[18] The cycling performance of Co_3O_4 nanosheets for lithium storage at a current density of 0.2 A g^{-1} is shown in Figure 3b. The first discharge capacity is 1797 mA h g^{-1}, followed by a high reversible charge capacity of 1173 mA h g^{-1}. Thus the initial coulombic efficiency reaches 65.3% and stabilizes at ~ 99% after 1st cycle. As mentioned previously, the irreversible capacity loss generally results from the SEI layer and/or electrolyte decomposition. No obvious capacity decay in subsequent cycles is observed, and the cell keeps a high capacity retention of 1029 mA h g^{-1} after 100 cycles. The cycling performance is competitive compared to some other Co_3O_4 electrodes with complexed nanostructures or carbonaceous materials modified Co_3O_4 composites, such as carbon-doped Co_3O_4 hollow nanofibers (1121 mA h g^{-1} after 100 cycles at 200 mA g^{-1}),[19] and carbon-encapsulated Co_3O_4 nanoparticles (1413 mA h g^{-1} at 100 mA g^{-1} after 100 cycles).[20]

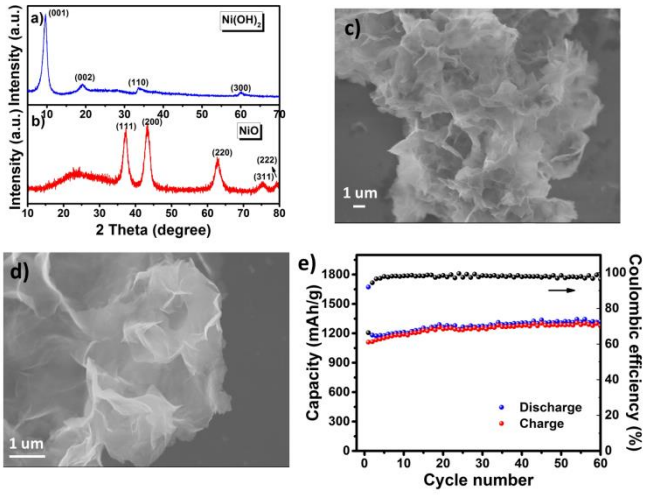

Figure 4. XRD patterns of as-prepared products: (a) $Ni(OH)_2$ and (b) NiO. SEM images of as-prepared products: (c) $Ni(OH)_2$ and (d) NiO. (e) Cycling performance of NiO nanosheets as anode materials of LIB in the voltage window of 0.001-3.0 V (vs. Li/Li^+) at a current density of 200 mA g^{-1}.

Based on the successful synthesis of $Co(OH)_2$ and Co_3O_4 nanosheets, some other analogue nanosheets including binary and ternary transition metal oxides (NiO and $NiCo_2O_4$) were also prepared by the same synthesis procedure, and their electrochemical performances as anodes for LIBs were preliminarily evaluated. As shown in Figure 4a, *α*-NiOH with a hexagonal layered structure (JCPDS Card No.22-0444) was acquired by the solvothermal process at 120 °C for 4h. The SEM image in Figure 4c shows a 2D sheet-like structure of *α*-NiOH. The *α*-NiOH nanosheets are uniform and exhibit gauze-like morphology. NiO nanosheets were obtained after the same heat treatment process as Co_3O_4, which can be indexed to a cubic phase structure (JCPDS Card No. 47-1409) as shown in Figure 4b. NiO inherits the morphology of *α*-NiOH nanosheets. As a proof-of-concept application, the lithium storage performance of NiO nanosheets is demonstrated. The NiO nanosheets deliver a high charge capacity of 1109 mA h g^{-1} with an initial coulombic efficiency of 66.3%. As presented in Figure

4e, the NiO nanosheet electrode shows excellent cycling stability at 200 mA g^{-1}, and a high specific capacity of 1314 mA h g^{-1} is sustained with a relatively high coulombic efficiency of ~ 99% over 60 cycles. $NiCo_2O_4$ possesses a spinel structure with Ni occupying the octahedral sites and Co occupying both tetrahedral and octahedral sites. Given Ni and Co exhibit a mixture of oxidation states, $NiCo_2O_4$ possesses much higher electrical conductivity than NiO and Co_3O_4, and this unique property makes $NiCo_2O_4$ very attractive towards energy storage/conversion and catalysis applications.[21] $Ni(OH)_2$-$Co(OH)_2$ (denoted as $NiCo_2(OH)_6$) solid solution was firstly prepared as precursor to synthesize $NiCo_2O_4$ nanosheets by the similar process. The hydroxide solid-solution keeps the hexagonal layered structure, as shown in Figure 5a. It can be observed that the as-prepared $NiCo_2(OH)_6$ also exhibits very flexible sheet-like 2D morphology (Figure 5c). After annealing in air at 300 °C for 2 h, cubic $NiCo_2O_4$ is obtained as shown in Figure 5b (JCPDF Card No. 20-0781). The $NiCo_2O_4$ maintains the ultrathin 2D nanosheet structure as well as large in-plane area of up to several microns. As shown in Figure 5d, $NiCo_2O_4$ nanosheet electrode shows considerably stable cycling performance for lithium storage, delivering 1346 mAh g^{-1} during the 60th cycle at 200 mA g^{-1}. The encouraging lithium storage performances of NiO and $NiCo_2O_4$ nanosheets further confirms the unique superiority of 2D nanomaterials for energy storage applications.

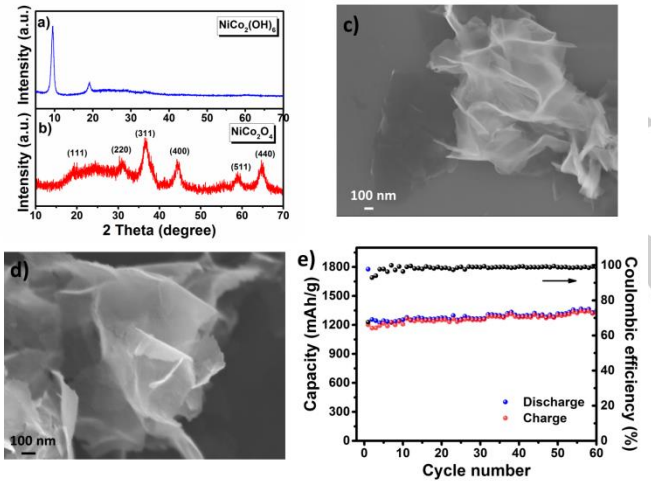

Figure 5. XRD patterns of as-prepared products: (a) $NiCo_2(OH)_6$ and (b) $NiCo_2O_4$. SEM images of as-prepared products: (c) $NiCo_2(OH)_6$ and (d) $NiCo_2O_4$. (e) Cycling performance of $NiCo_2O_4$ nanosheets as anode materials of LIB in the voltage window of 0.001-3.0 V (vs. Li/Li^+) at a current density of 200 mA g^{-1}.

Conclusions

In summary, a universal and scalable process was developed to prepare Ni/Co-based hydroxide and oxide nanosheets. The performances of the oxide nanosheets as anodes for rechargeable batteries were investigated. Benefiting from the unique properties of the 2D morphology, the Co_3O_4 nanosheets exhibit very impressive sodium (150 mA h g^{-1} at 10.0 A g^{-1}, and 404 mA h g^{-1} after 100 cycles at 0.1 A g^{-1}) and lithium (1029 mA h g^{-1} after 100 cycles at 0.2 A g^{-1}) storage capabilities with high specific capacity, good rate capability and cycling life. As a proof-of-concept, the performances of NiO and $NiCo_2O_4$ nanosheets were also evaluated as anodes for LIBs, and both materials delivered high-capacity and durable lithium storage performances (1314 and 1346 mAh g^{-1} for NiO and $NiCo_2O_4$, respectively, after 60 cycles at 0.2 A g^{-1}). The present results demonstrate the great potential of 2D metal oxide nanomaterials for energy storage/conversion-related applications.

Experimental Section

Synthesis of Ni/Co-based hydroxides and oxides nanosheets

In a typical synthesis of cobalt hydroxide and Co_3O_4 nanosheets, 1.8 mmol $Co(NO_3)_2{\cdot}6H_2O$ and 3.6 mmol hexamethylene tetramine (HMT) were firstly dissolved in a mixed solvent containing 16 mL deionized water and 24 mL ethylene glycol (EG) under vigorous stirring. Consequently, the pink solution was transferred to a Teflon lined stainless-steel autoclave with a capacity of 50 mL. The autoclave was sealed and maintained at 120 °C for 4 h in an electric oven. The autoclave cooled down naturally after reaction, and light green products were collected by centrifugation followed by repeated washing with deionized water. Finally, the products were freeze-dried for two days, obtaining cobalt hydroxide nanosheets. Co_3O_4 nanosheets were obtained by annealing the cobalt hydroxide nanosheets in air at 300 °C for 2 h with a heating rate of 5 °C min^{-1}. For the synthesis of nickel hydroxide and NiO nanosheets, the experimental procedure was the same as the aforementioned steps except that the metal ion precursor was 1.8 mmol $Ni(NO_3)_2{\cdot}6H_2O$. For the synthesis of nickel/cobalt hydroxide and $NiCo_2O_4$ nanosheets, 0.6 mmol $Ni(NO_3)_2{\cdot}6H_2O$ and 1.2 mmol $Co(NO_3)_2{\cdot}6H_2O$ were used as the metal ion precursors. The hydroxide precursors were annealed in air at 300 °C for 2 h to obtain the oxide counterparts.

Materials characterization

The phase and surface chemical state were determined by X-ray diffraction (XRD, MMA GBC, Australia). The morphology of the as-prepared products was observed by a JEOL JSM-7500FA field-emission scanning electron microscope (FESEM) and a JEOL 2010 transmission electron microscope (TEM). Hermogravimetric analysis (TGA, Q500) was carried out from room temperature to 450 °C at a heating rate of 10 K min^{-1} in air.

Electrochemical measurements

The active material (Co_3O_4, NiO, or $NiCo_2O_4$ nanosheets) was thoroughly mixed with carbon nanotubes (CNTs) and poly(vinyl difluoride) (PVDF) at a weight ratio of 7:2:1 in N-methylpyrrolidone solvent to form a homogeneous slurry. The cell working electrodes were prepared by painting the slurry on copper foil, followed by vacuum drying at 80 °C overnight. The coin-type half-cells were assembled in an Ar-filled glove box with both H_2O and O_2 levels less than 1 ppm. For SIBs, metallic Na foil was employed as the counter/reference electrode, and Whatman GF/D microfiber filter paper was used as the separator.

1 M $NaClO_4$ dissolved in propylene carbonate (PC) with 5% fluoroethylene carbonate (FEC) additive was chosen as the electrolyte. For LIBs, lithium foils were used as counter/reference electrodes. Celgard 2400 membrane was used as separator, and 1 M $LiPF_6$ dissolved in ethylene carbonate (EC)/dimethyl carbonate (DMC) (1/1, w/w) was used as electrolyte. Galvanostatic charge/discharge testing was conducted in the voltage range of 0.01-3.0 V using a NEWARE multichannel battery test system.

Acknowledgements

This work was financially supported by Australian Research Council (ARC) DECRA Grant (DE160100596) and ARC Discovery Project (DP160102627). Y.Z. Jiang acknowledges support from the National Natural Science Foundation of China (Grant No. 21373184) and the Public Projects of Zhejiang Province (2015C31039).

Keywords: Nanosheets · Transition metal oxide · Anode · Sodium ion batteries · Lithium ion batteries

[1] a) D. C. Tsui, T. Englert, A. Y. Cho and A. C. Gossard, *Phy. Rev. Lett.* **1980**, *44*, 341-344; b) P. K. Kannan, D. J. Late, H. Morgan and C. S. Rout, *Nanoscale* **2015**, *7*, 13293-13312; c) Y. H. Hu, H. Wang and B. Hu, *Chemsuschem* **2010**, *3*, 782-796; d) J. H. Liu and X. W. Liu, *Adv. Mater.* **2012**, *24*, 4097-4111.

[2] a) W.-B. Luo, S.-L. Chou, J.-Z. Wang, Y.-M. Kang, Y.-C. Zhai and H.-K. Liu, *Chemical Communications* **2015**, *51*, 8269-8272; b) X. Huang, Z. Y. Yin, S. X. Wu, X. Y. Qi, Q. Y. He, Q. C. Zhang, Q. Y. Yan, F. Boey and H. Zhang, *Small* **2011**, *7*, 1876-1902; c) Y. Q. Sun, Q. O. Wu and G. Q. Shi, *Energy Environ. Sci.* **2011**, *4*, 1113-1132.

[3] a) H. T. Tan, W. Sun, L. Wang and Q. Yan, *ChemNanoMat* **2016**, *2*, 562-577; b) G. Zhang, H. J. Liu, J. H. Qu and J. H. Li, *Energy Environ. Sci.* **2016**, *9*, 1190-1209; c) C. L. Tan and H. Zhang, *Nat. Commun.* **2015**, *6*, 1-13; d) M. R. Kaiser, X. Liang, K. Konstantinov, H.-K. Liu, S.-X. Dou and J.-Z. Wang, *Chemistry-a European Journal* **2015**, *21*, 10061-10069; e) Z. Sun, T. Liao, Y. Dou, S. M. Hwang, M. S. Park, L. Jiang, J. H. Kim and S. X. Dou, *Nat. Commun.* **2014**, *5*, 1-9.

[4] a) M. D. Slater, D. Kim, E. Lee and C. S. Johnson, *Adv. Funct. Mater.* **2013**, *23*, 947-958; b) N. Yabuuchi, K. Kubota, M. Dahbi and S. Komaba, *Chem. Rev.* **2014**, *114*, 11636-11682; c) Z. G. Yang, J. L. Zhang, M. C. W. Kintner-Meyer, X. C. Lu, D. W. Choi, J. P. Lemmon and J. Liu, *Chem. Revi.* **2011**, *111*, 3577-3613; d) B. Dunn, H. Kamath and J. M. Tarascon, *Science* **2011**, *334*, 928-935; e) S. Yuan, S. Wang, L. Li, Y. H. Zhu, X. B. Zhang and J. M. Yan, *ACS Appl. Mater. Interfaces* **2016**, *8*, 9178-9184; f) S. Wang, S. Yuan, Y.-B. Yin, Y.-H. Zhu, X.-B. Zhang and J.-M. Yan, *Part. Part. Syst. Charact.* **2016**, *33*, 493-499; g) X. Wang, Y. Chen, O. G. Schmidt and C. Yan, *Chem. Soc. Rev.* **2016**, *45*, 1308-1330.

[5] a) J. Jiang, Y. Y. Li, J. P. Liu, X. T. Huang, C. Z. Yuan and X. W. Lou, *Adv. Mater.* **2012**, *24*, 5166-5180; b) M. V. Reddy, G. V. S. Rao and B. V. R. Chowdari, *Chem. Rev.* **2013**, *113*, 5364-5457; c) C. B. Zhu, X. K. Mu, P. A. van Aken, Y. Yu and J. Maier, *Angew. Chem. Int. Ed.* **2014**, *53*, 2152-2156; d) R. Alcantara, M. Jaraba, P. Lavela and J. L. Tirado, *Chem. Mater.* **2002**, *14*, 2847-2848; e) L. David, R. Bhandavat and G. Singh, *ACS Nano* **2014**, *8*, 1759-1770.

[6] a) W. Sun, X. Rui, D. Yang, Z. Sun, B. Li, W. Zhang, Y. Zong, S. Madhavi, S. Dou and Q. Yan, *Acs Nano* **2015**, *9*, 11371-11381; b) Y. Jiang, D. Zhang, Y. Li, T. Yuan, N. Bahlawane, C. Liang, W. Sun, Y. Lu and M. Yan, *Nano Energy* **2014**, *4*, 23-30.

[7] a) W. Sun, X. Rui, J. Zhu, L. Yu, Y. Zhang, Z. Xu, S. Madhavi and Q. Yan, *J. Power Sources* **2015**, *274*, 755-761; b) J. Wang, J. Liu, H. Yang, D. Chao, J. Yan, S. V. Savilov, J. Lin and Z. X. Shen, *Nano Energy* **2016**, *20*, 1-10; c) J. S. Cho, J. K. Lee and Y. C. Kang, *Sci. Rep.* **2016**, *6*, 23699-23711; d) Y. J. Zhai, H. Z. Mao, P. Liu, X. C. Ren, L. Q. Xu and Y. T. Qian, *J. Mater. Chem. A* **2015**, *3*, 16142-16149.

[8] a) X.-l. Huang, R.-z. Wang, D. Xu, Z.-l. Wang, H.-g. Wang, J.-j. Xu, Z. Wu, Q.-c. Liu, Y. Zhang and X.-b. Zhang, *Adv. Funct. Mater.* **2013**, *23*, 4345-4353; b) X.-l. Huang, J. Chai, T. Jiang, Y.-J. Wei, G. Chen, W.-q. Liu, D. Han, L. Niu, L. Wang and X.-b. Zhang, *J. Mater. Chem.* **2012**, *22*, 3404; c) X.-l. Huang, X. Zhao, Z.-l. Wang, L.-m. Wang and X.-b. Zhang, *J. Mater. Chem.* **2012**, *22*, 3764; d) T. Yang, T. Qian, M. Wang, X. Shen, N. Xu, Z. Sun and C. Yan, *Adv. Mater.* **2016**, *28*, 539-545.

[9] a) S. Das, M. Kim, J.-w. Lee and W. Choi, *Criti. Rev. Solid State* **2014**, *39*, 231-252; b) C. L. Tan and H. Zhang, *Chem. Soc. Rev.* **2015**, *44*, 2713-2731.

[10] a) K. Varoon, X. Zhang, B. Elyassi, D. D. Brewer, M. Gettel, S. Kumar, J. A. Lee, S. Maheshwari, A. Mittal, C. Y. Sung, M. Cococcioni, L. F. Francis, A. V. McCormick, K. A. Mkhoyan and M. Tsapatsis, *Science* **2011**, *334*, 72-75; b) V. Nicolosi, M. Chhowalla, M. G. Kanatzidis, M. S. Strano and J. N. Coleman, *Science* **2013**, *340*, 1420-1437; c) J. N. Coleman, M. Lotya, A. O'Neill, S. D. Bergin, P. J. King, U. Khan, K. Young, A. Gaucher, S. De, R. J. Smith, I. V. Shvets, S. K. Arora, G. Stanton, H. Y. Kim, K. Lee, G. T. Kim, G. S. Duesberg, T. Hallam, J. J. Boland, J. J. Wang, J. F. Donegan, J. C. Grunlan, G. Moriarty, A. Shmeliov, R. J. Nicholls, J. M. Perkins, E. M. Grieveson, K. Theuwissen, D. W. McComb, P. D. Nellist and V. Nicolosi, *Science* **2011**, *331*, 568-571.

[11] a) W.-J. Li, S.-L. Chou, J.-Z. Wang, Y.-M. Kang, J.-L. Wang, Y. Liu, Q.-F. Gu, H.-K. Liu and S.-X. Dou, *Chem. Mater.* **2015**, *27*, 1997-2003; b) A. Reina, X. T. Jia, J. Ho, D. Nezich, H. B. Son, V. Bulovic, M. S. Dresselhaus and J. Kong, *Nano Lett.* **2009**, *9*, 30-35; c) Y. H. Lee, X. Q. Zhang, W. J. Zhang, M. T. Chang, C. T. Lin, K. D. Chang, Y. C. Yu, J. T. W. Wang, C. S. Chang, L. J. Li and T. W. Lin, *Adv. Mater.* **2012**, *24*, 2320-2325.

[12] S. Jeong, D. Yoo, J.-t. Jang, M. Kim and J. Cheon, *J. Am. Chem. Soc.* **2012**, *134*, 18233-18236.

[13] M. M. Rahman, A. M. Glushenkov, T. Ramireddy and Y. Chen, *Chemi. Commun.* **2014**, *50*, 5057-5060.

[14] J. Vetter, P. Novák, M. R. Wagner, C. Veit, K. C. Möller, J. O. Besenhard, M. Winter, M. Wohlfahrt-Mehrens, C. Vogler and A. Hammouche, *J. Power Sources* **2005**, *147*, 269-281.

[15] Z. Jian, P. Liu, F. Li, M. Chen and H. Zhou, *J. Mater. Chem. A* **2014**, *2*, 13805-13809.

[16] W. K. Pang, S. Kalluri, V. K. Peterson, N. Sharma, J. Kimpton, B. Johannessen, H. K. Liu, S. X. Dou and Z. Guo, *Chemistry of Materials* **2015**, *27*, 3150-3158.

[17] Y. Wang, C. Wang, Y. Wang, H. Liu and Z. Huang, *J. Mater. Chem. A* **2016**, *4*, 5428-5435.

[18] K. He, F. Lin, Y. Zhu, X. Yu, J. Li, R. Lin, D. Nordlund, T. C. Weng, R. M. Richards, X. Q. Yang, M. M. Doeff, E. A. Stach, Y. Mo, H. L. Xin and D. Su, *Nano Lett.* **2015**, *15*, 5755-5763.

[19] C. Yan, G. Chen, X. Zhou, J. Sun and C. Lv, *Adv. Funct. Mater.* **2016**, *26*, 1428-1436.

[20] X. Leng, S. Wei, Z. Jiang, J. Lian, G. Wang and Q. Jiang, *Sci. Rep.* **2015**, *5*, 16629-16639.

[21] a) G. Q. Zhang, H. B. Wu, H. E. Hoster, M. B. Chan-Park and X. W. Lou, *Energy Environ. Sci.* **2012**, *5*, 9453; b) S. Abouali, M. A. Garakani, Z. L. Xu and J. K. Kim, *Carbon* **2016**, *102*, 262-272; c) L. L. Liu, J. Wang, Y. Y. Hou, J. Chen, H. K. Liu, J. Z. Wang and Y. P. Wu, *Small* **2016**, *12*, 602-611.

Entry for the Table of Contents

Layout 1:

FULL PAPER

A universal process that can be extended to scale-up is developed for synthesizing ultrathin Co/Ni-based hydroxides and oxides. For sodium storage, the Co_3O_4 nanosheets exhibit excellent rate capability (e.g. 179 mA h g^{-1} at 7.0 A $g^{-1}$and 150 mA h g^{-1} at 10.0 A g^{-1}) and promising cycling performance (404 mA h g^{-1} after 100 cycles at 0.1 A g^{-1}).

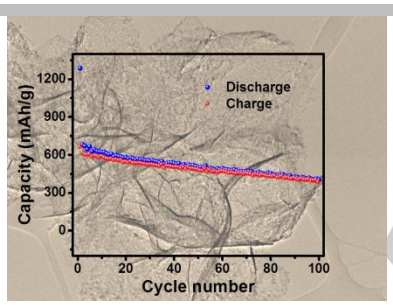

Dan Zhang,[a,b] Wenping Sun,[a] Yu Zhang,[a] Wenbin Luo,[a] Yinzhu Jiang,*[b] Shi Xue Dou[a]*

Page No. – Page No.

Two-dimensional Cobalt/Nickel-Based Oxide Nanosheets for High-Performance Sodium and Lithium Storage